Supporting Information

Buchli et al. 10.1073/pnas.1306323110

SI Text

IR-Data

The amide I band was used to observe changes in the protein backbone structure. Additionally, two bands originating from the photoswitch (see Fig. S1*A*), present in the absolute FTIR spectrum in Fig. S2*A* (blue), are sensitive to the photoswitch conformational state. The band at around 1,390 cm^{-1} is a ring mode of the azobenzene and at around 1,490 cm^{-1} is the amide II band of the two photoswitch amide groups (Fig. S1*A*). In the absolute spectra of the photoswitch bound to the protein (Fig. S2*B*, blue), these two modes are hidden behind the stronger amide II band of the protein backbone, but they still are clearly visible in the difference spectra (Fig. S2*B*, red and green), where they appear in a similar way to that for the photoswitch alone (Fig. S2*A*, red and green).

Fig. 3 (blue) of the main text shows a time trace of the photoswitch amide II band. Shortly following the heat signal decay within the first few picoseconds, the spectrum quickly relaxes to closely resemble the steady-state spectrum (Fig. 3 and Fig. S2*A*). When the photoswitch is bound to the second PDZ (PDZ2), both bands overlap with the much broader amide II band of the protein backbone (centered around 1,450 cm^{-1}; Fig. S 1*B*, blue); however, the bands originating from the photoswitch are clearly discernible in the difference spectrum. The kinetics are significantly decelerated by the counterstrain the protein imposes onto the photoswitch.

Table S1 summarizes all parameters obtained from the joint fit of the data in Fig. 3.

SI Materials and Methods

Cloning. The PDZ2 gene, containing the two mutations S21C and E76C, was synthesized and cloned into a pET30a(+)vector (EZbiolab). A human rhinovirus 3C (HRV 3C) cleavage site was added between the N-terminal hexahistidine tag and the protein gene by site-directed mutagenesis (QuikChange; Stratagene). To facilitate detection and quantification of the protein vs. the photoswitchable linker, a Trp was inserted between the His tag and the protease cleavage site (Fig. S2*B*).

Protein Expression and Purification. For IR spectroscopy measurements, the PDZ2 domain was expressed in *Escherichia coli* BL21(DE3) in Luria–Bertani medium. For NMR measurements, M9 minimal medium was supplemented with ^{13}C-glucose and/or ^{15}N-NH_4Cl. Fractional isotope labeling as described by Neri et al. (2) was used for obtaining stereospecific assignments for the Val and Leu methyl groups. The protein was purified from inclusion bodies with a HisPrep column (GE Healthcare Life Sciences) in 20 mM Tris·HCl, 6 M GdmHCl, and 10 mM imidazole, pH 8, and eluted with an imidazole gradient. Residual nickel was removed from the protein by incubation with 40 mM EDTA at 4 °C for at least 12 h.

Linking the Photoswitch to PDZ2. The 3,3′-bis(sulfonato)-4,4′-bis (chloroacetamido)azobenzene (BSBCA) (Fig. S1*A*) was synthesized according to the protocol from Burns et al. (1). The process to covalently link the photoswitch to two surface-exposed Cys residues, as outlined in the protocol, was modified to the following: Disulfide bridges were reduced by adding 50 mM DTT to the protein solution and incubating it for at least 1 h at room temperature. The protein was then refolded by desalting in 50 mM Tris·HCl, pH 8.5, with a HiPrep column (GE Healthcare Life Sciences), simultaneously removing the reducing agent. To prevent the reformation of disulfide bonds, fraction collection was performed in an oxygen-free (argon) atmosphere. The protein was then diluted with a well-degassed buffer (50 mM Tris·HCl, pH 8.5) to 10 μM before 50 μM of BSBCA was added, still under Ar atmosphere. The reaction vessel was sealed and stirred in the dark for 6 h. The reaction mixture was concentrated using a Vivacell pressure concentrator with a 5-kDa MWCO filter (Sartorius). To remove any surplus BSBCA the protein solution was diluted and reconcentrated twice. The monomer with a single photoswitch correctly linked to both Cys was purified using a MonoQ anion exchange column (GE Healthcare Life Sciences) in 50 mM Tris·HCl, pH 8.5, and eluted with an NaCl gradient.

His Tag Cleavage. After linking the photoswitch (BSBCA) to PDZ2, the His tag was removed with HRV 3C protease. The protease used also contained a His tag for separation from the sample. One milligram protease per 50 mg PDZ2 in 50 mM Tris·HCl, pH 8.5, was incubated at 4 °C for 16 h. The His tag-free PDZ2 was purified with a HisTrap column (GE Healthcare Life Sciences) and the buffer was exchanged by a HiPrep desalting column (GE Healthcare Life Sciences) to the corresponding buffer used for IR or NMR measurements.

Mass Spectrometry. Electrospray ionization (ESI) mass spectra were measured at the Functional Genomics Center Zurich in a mass range between 500 and 3,000 Da. The *m*/*z* data were deconvolved using the MasEnt1 software.

The purity of all samples was verified by SDS/PAGE (Fig. S3) and ESI mass spectrometry (Fig. S4*A*). Additionally, ESI mass spectra were repeated after time-resolved IR measurements. Thereby, we realized that the protein was modified during a measurement in Tris buffer (Fig. S4*B*). However, these modifications could be largely avoided by measuring in borate buffer and under exclusion of oxygen (Fig. S4*C*). All transient IR spectra shown in this work were therefore measured under these conditions.

Fig. S4*B* shows one modification with an increased mass of around 16 Da that can occur multiple times. We attribute this to an oxidation of the protein, most likely at the thioether groups of the cysteines linked to the photoswitch. A small part of the protein was already oxidized before the measurement (Fig. S4*A*). However, during a measurement the oxidation significantly increased. A second modification with an increased mass of 135 Da we attribute to a reaction of the oxidized protein with the Tris buffer. Both modifications increased linearly with the time of a measurement and must have been induced by the high intensity of the 420-nm laser pulses. No decomposition products with a lighter mass were detected.

IR Spectroscopy. For FTIR measurements the protein was desalted into 50 mM Tris·HCl, 150 mM NaCl, pH 8.5. We learned that in this buffer the protein is modified under the influence of 420-nm laser pluses (mass spectra, Fig. S4). Therefore, we used 50 mM borate buffer and 150 mM NaCl, pH 8.5, for time-resolved measurements. The protein was concentrated in an Amicon Ultra 3-kDa MWCO centrifugal filter device (Millipore Corporation) to 1.3 mM, lyophilized, and dissolved in D_2O. Incubation in D_2O for 2 h at room temperature before the measurements eliminated H/D exchange during experiments. FTIR spectra were measured on a Bruker Tensor 27 FTIR spectrometer in

a 50-μm or 100-μm path-length sample cell with CaF_2 windows, either in the dark or under illumination with a 150-mW, 370-nm continuous wave (cw) diode laser (CrystaLaser). The unlinked photoswitch (Figs. 1*A* and 3) was measured in the same buffer and at 1.1 mM concentration.

All FTIR and transient IR spectra were measured at room temperature (21–22 °C).

NMR Spectroscopy. For NMR spectroscopy the samples (in 50 mM sodium phosphate, 150 mM NaCl, pH 6.8) were concentrated to 0.75 mM. The buffer was exchanged (50 mM sodium phosphate, pH 6.8, 150 mM NaCl, 10% D_2O) in two successive rounds of 1:1 dilution and concentration. For measurements with the photoswitch *in cis* a 150-mW, 370-nm cw diode laser (CrystaLaser) coupled to a fiber with a custom-designed inline radial illumination probe (Polymicro Technologies) (Fig. S5) was used.

Proton chemical shifts were calibrated to the water signal and nitrogen shifts were referenced indirectly to liquid NH_3 (3). All 2D experiments used TPPI-States for quadrature detection in indirect proton dimensions and gradient-selected coherence selection (echo–antiecho) (4) in combination with sensitivity enhancement schemes in experiments including detection of amide protons.

Resonance Assignment. All NMR experiments were recorded at 25 °C on a Bruker Avance 600- or 700-MHz spectrometer equipped with a cryoprobe. Backbone resonances were identified with the help of CBCA(CO)NH (5), HNCACB (6), and HNCO (7) experiments. Side-chain assignments were obtained using HC(C)H-TOCSY (8, 9) and CC(CO)NH (10) experiments. Aromatic spin systems were linked to the backbone via a CB(CGCD)HD experiment (11). Val and Leu methyl groups were stereospecifically assigned (2). Spectra were processed under the Bruker Topspin 2.1 software and then transferred to Cara (12) for further analysis. The overall backbone/sidechain assignment completeness is 98/85% and 96/84% for the *cis* and *trans* forms, respectively. The lower percentage of backbone resonance assignments of the *trans* form is due to a bigger number of exchange-broadened peaks in proximity to the linker attachment points.

Structure Calculation. ^{15}N- and ^{13}C-edited NOESY (13) spectra with mixing times of 75 ms were used for obtaining NOE structural restraints. Two sets of amide proton residual dipolar couplings (NH-RDCs) (14) were measured for both the *cis* and the *trans* form in 8.5 mg/mL filamentous phage Pf1 (15) (ASLA Biotech) and in liquid crystalline media formed with *n*-dodecyl-penta(ethylene glycol) (C12E5) and *n*-hexanol (16). NOESY peaks were picked with ATNOS/CANDID (17, 18). Torsion angle restraints were generated with TALOS+ (19) and final structures were calculated with CYANA (20, 21). For the *trans* form a number of artificial restraints were imposed on the photoswitch to enforce a *trans*-diazo bond and coplanar aromatic rings whereas for the *cis* form only the *cis*-diazo bond was enforced (Table S2).

Structure Refinement. Structures were refined in TIP3P (three-site transferrable intermolecular potential) explicit water, using the Charmm27 force field as described previously (22–24). Parameters for the BSBCA cross-linker were derived by analogy as for azobenzene (25, 26). The structures of the *cis* and the *trans* form both show the β6/α2 architecture characteristic of PDZ2 domains. The *trans* form suffers from a number of exchange-broadened peaks, in particular in the β1-β2 loop resulting in low numbers of available distance restraints for that region concomitant with a less well-defined structure in that stretch compared with the overall structure. We point out here that the determination of the NMR structures relies on a force field similar to the one used for carrying out the molecular dynamics (MD) simulations and that distance values determined from the two methods might thus be not fully independent.

Structure Validation. Structures were validated with WHATCHECK (27, 28) and PROCHECK-NMR (29) (Table S3).

Data Bank Accession Codes. Coordinates and chemical shifts of the *cis* and *trans* configurations have been deposited in the Protein Data Bank (PDB) and the BioMagResBank (BMRB) data bank under PDB ID codes 2M0Z and 2M10 and BMRB accession nos. 18833 and 18834, respectively.

Computation. MD simulations were performed with the Gromacs program package (30) and the Gromacs implementation of the Charmm27 force field (23, 24), with a timestep of 2 fs, saving time 500 fs, all bonds constrained, isothermal–isobaric (NPT) ensemble at 300 K and 1 bar, with time constants of 0.2 ps and 0.5 ps, respectively, for the thermostat and the barostat. Lennard–Jones interactions were treated with a cutoff of 1.0 nm (switched to zero at 0.9 nm), and the long-range electrostatic forces were approximated by the Particle–Mesh–Ewald approximation. The photoswitch was parameterized as in refs. 25 and 26. To force the photoswitch to be either in the *cis* or in the *trans* configuration, the double-minimum potential for the central C-N = N-C dihedral angle was replaced by a single-minimum potential, and the force constant was increased by a factor of 3 such that the potential around the minimum agrees reasonably well with that of the original double-minimum potential from refs. 31 and 32.

PDB entry 3PDZ was used as a starting structure (33) and mutated to Ser21Cys and Glu76Cys to provide an anchor point for the photoswitch. In addition, a Tyr36Trp mutation was included in accordance with an earlier version of the experimental sequence. We inserted a photoswitch without the sulfonate groups. We were able to synthesize proteins with that version of the photoswitch in small yields and verified that despite its hydrophobicity, the protein was still folded (however, the yields of the synthesis were too small to retrieve enough material for NMR and time-resolved IR spectroscopy).

As in the experiment, we first prepared the photoswitch in its *cis* configuration. The protein was solvated in a box of 5,355 TIP3P water molecules and one Cl^- counter-ion to neutralize the simulation box, minimized with the backbone atoms constrained, and then equilibrated for 1.1 μs. From a subsequent 3-μs *cis*-equilibrium simulation, 300,000 snapshots separated by 10 ps each were taken as starting points for the nonequilibrium MD runs with the photoswitch switched into *trans*. Simulation times varied between 4 ps and 100 ns such that the number of samples in each time bin on a logarithmic time axis was roughly the same. That is, we ran 150,000 trajectories for 4 ps, 75,000 trajectories for 8 ps, and so on, up to 73 trajectories for 8 ns. In addition, 120 trajectories for a full 100 ns were collected. The total simulation time of these nonequilibrium trajectories amounts to ~21 μs and took about 5 months on a 96-core computer cluster. Both Figs. 4 and 5 are calculated from that full set of nonequilibrium trajectories.

To calculate the water density on the protein surface (Fig. 5 and Movie S1), the 300,000 starting points, which resemble a *cis*-equilibrium ensemble, were aligned on each other by minimizing the rmsd of the C_α atoms from ordered secondary structure motives. An averaged structure was calculated from these starting points by averaging atom positions, which served as a reference to which all subsequent nonequilibrium structures were aligned together with their surrounding water molecules. The positions of the water-oxygens were then binned into cubes of 1 $Å^3$.

The residence times of water molecules were estimated by computing the average lifetime of individual water/protein hydrogen bonds along a 600-ns equilibrium MD trajectory with the photoswitch *in trans*. Time series of presence/rupture of individual hydrogen bonds were obtained by Gromacs with default thresholds of 0.35 nm for the donor–acceptor distance and 30°

for the acceptor–donor–hydrogen angle. Seven hydrogen bond donor or acceptor groups within the binding groove and 13 on the outside surface were used. Averaging over these groups resulted in hydrogen bond lifetimes of 40 ± 20 ps within the binding groove and 15 ± 5 ps on the outside surface. Neglecting transient hydrogen bond ruptures up to 10 ps yielded residence times of 60 ± 50 ps within the binding groove and 20 ± 10 ps on the outside surface.

The implicit solvent simulations were carried out according to a similar protocol with Newtonian dynamics at 300 K, using a generalized Born formalism (34). A *cis* structure already equilibrated in explicit solvent was further equilibrated for 300 ns in implicit solvent. A 700-ns production equilibrium run was then used to collect an ensemble of initial structures every 10 ns for the subsequent nonequilibrium simulations.

1. Burns DC, Zhang F, Woolley GA (2007) Synthesis of 3,3′-bis(sulfonato)-4,4′-bis (chloroacetamido)azobenzene and cysteine cross-linking for photo-control of protein conformation and activity. *Nat Protoc* 2(2):251–258.
2. Neri D, Szyperski T, Otting G, Senn H, Wüthrich K (1989) Stereospecific nuclear magnetic resonance assignments of the methyl groups of valine and leucine in the DNA-binding domain of the 434 repressor by biosynthetically directed fractional 13C labeling. *Biochemistry* 28(19):7510–7516.
3. Live DH, Davis DG, Agosta WC, Cowburn D (1984) Observation of 1000-fold enhancement of nitrogen-15 NMR via proton-detected multiquantum coherences: Studies of large peptides. *J Am Chem Soc* 106(20):6104–6105.
4. Kay LE, Keifer P, Saarinen T (1992) Pure absorption gradient enhanced heteronuclear single quantum correlation spectroscopy with improved sensitivity. *J Am Chem Soc* 114(26):10663–10665.
5. Grzesiek S, Bax A (1992) Correlating backbone amide and side chain resonances in larger proteins by multiple relayed triple resonance nmr. *J Am Chem Soc* 114:6291–6293.
6. Grzesiek S, Bax A (1992) An efficient experiment for sequential backbone assignment of medium-sized isotopically enriched proteins. *J Magn Reson* 99:201–207.
7. Kay LE, Ikura M, Tschudin R, Bax A (1990) Three-dimensional triple-resonance NMR spectroscopy of isotopically enriched proteins. *J Magn Reson* 89:496–514.
8. Kay LE, Ikura M, Bax A (1990) Proton-proton correlation via carbon-carbon couplings: A three-dimensional NMR approach for the assignment of aliphatic resonances in proteins labeled with carbon-13. *J Am Chem Soc* 112:888–889.
9. Ikura M, Kay LE, Bax A (1991) Improved three-dimensional 1H-13C-1H correlation spectroscopy of a 13C-labeled protein using constant-time evolution. *J Biomol NMR* 1(3):299–304.
10. Grzesiek S, Anglister J, Bax A (1993) Correlation of backbone amide and aliphatic side-chain resonances in 13C/15N-enriched proteins by isotropic mixing of 13C magnetization. *J Magn Reson* 101(1):114–119.
11. Yamazaki T, Forman-Kay JD, Kay LE (1993) 2-dimensional NMR experiments for correlating C-13-beta and H-1-delta/epsilon chemical-shifts of aromatic residues in C-13-labeled proteins via scalar couplings. *J Am Chem Soc* 115:11054–11055.
12. Keller RL (2004) *The Computer Aided Resonance Tutorial* (Cantina).
13. Marion D, Kay LE, Sparks SW, Torchia DA, Bax A (1989) Three-dimensional heteronuclear NMR of nitrogen-15 labeled proteins. *J Am Chem Soc* 111(4):1515–1517.
14. Ottiger M, Delaglio F, Bax A (1998) Measurement of J and dipolar couplings from simplified two-dimensional NMR spectra. *J Magn Reson* 131(2):373–378.
15. Hansen MR, Hanson P, Pardi A (2000) Filamentous bacteriophage for aligning RNA, DNA, and proteins for measurement of nuclear magnetic resonance dipolar coupling interactions. *Methods Enzymol* 317:220–240.
16. Rückert M, Otting G (2000) Alignment of biological macromolecules in novel nonionic liquid crystalline media for nmr experiments. *J Am Chem Soc* 122(32): 7793–7797.
17. Herrmann T, Güntert P, Wüthrich K (2002) Protein NMR structure determination with automated NOE assignment using the new software CANDID and the torsion angle dynamics algorithm DYANA. *J Mol Biol* 319(1):209–227.
18. Herrmann T, Güntert P, Wüthrich K (2002) Protein NMR structure determination with automated NOE-identification in the NOESY spectra using the new software ATNOS. *J Biomol NMR* 24(3):171–189.
19. Shen Y, Delaglio F, Cornilescu G, Bax A (2009) TALOS+: A hybrid method for predicting protein backbone torsion angles from NMR chemical shifts. *J Biomol NMR* 44(4):213–223.
20. Güntert P, Mumenthaler C, Wüthrich K (1997) Torsion angle dynamics for NMR structure calculation with the new program DYANA. *J Mol Biol* 273(1):283–298.
21. Güntert P (2004) Automated NMR structure calculation with CYANA. *Methods Mol Biol* 278:353–378.
22. Spronk CAEM, Linge JP, Hilbers CW, Vuister GW (2002) Improving the quality of protein structures derived by NMR spectroscopy. *J Biomol NMR* 22(3):281–289.
23. Mackerell AD, Jr., Feig M, Brooks CL, 3rd (2004) Extending the treatment of backbone energetics in protein force fields: Limitations of gas-phase quantum mechanics in reproducing protein conformational distributions in molecular dynamics simulations. *J Comput Chem* 25(11):1400–1415.
24. Mackerell AD, et al. (1998) All-atom empirical potential for molecular modeling and dynamics studies of proteins. *J Phys Chem B* 102:3586–3616.
25. Spörlein S, et al. (2002) Ultrafast spectroscopy reveals subnanosecond peptide conformational dynamics and validates molecular dynamics simulation. *Proc Natl Acad Sci USA* 99(12):7998–8002.
26. Carstens H (2004) Konformationsdynamik lichtschaltbarer peptide: Molekulardynamiksimulationen und datengetriebene modellbildung [Conformational dynamics of photoswitchable peptides: Molecular dynamics and data-driven model building]. PhD thesis (Ludwig Maximilians Universität München, Munich). Available at http://edoc.ub.uni-muenchen.de/2268. German.
27. Vriend G (1990) WHAT IF: A molecular modeling and drug design program. *J Mol Graph* 8(1):52–56, 29.
28. Hooft RW, Vriend G, Sander C, Abola EE (1996) Errors in protein structures. *Nature* 381(6580):272.
29. Laskowski RA, Rullmannn JA, MacArthur MW, Kaptein R, Thornton JM (1996) AQUA and PROCHECK-NMR: Programs for checking the quality of protein structures solved by NMR. *J Biomol NMR* 8(4):477–486.
30. Van Der Spoel D, et al. (2005) GROMACS: Fast, flexible, and free. *J Comput Chem* 26(16):1701–1718.
31. Nguyen PH, Stock G (2006) Nonequilibrium molecular dynamics simulation of a photoswitchable peptide. *Chem Phys* 323:36–44.
32. Ihalainen JA, et al. (2008) α-Helix folding in the presence of structural constraints. *Proc Natl Acad Sci USA* 105(28):9588–9593.
33. Kozlov G, Gehring K, Ekiel I (2000) Solution structure of the PDZ2 domain from human phosphatase hPTP1E and its interactions with C-terminal peptides from the Fas receptor. *Biochemistry* 39(10):2572–2580.
34. Onufriev A, Bashford D, Case DA (2004) Exploring protein native states and large-scale conformational changes with a modified generalized born model. *Proteins* 55(2):383–394.

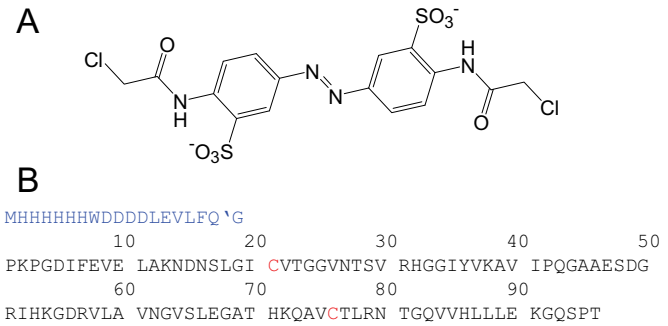

Fig. S1. Cross-linker and anchor sites in the protein sequence. (*A*) Photoswitch. This water-soluble thiol-reactive azobenzene derivative 3,3′-bis(sulfonato)-4,4′-bis(chloroacetamido)azobenzene (BSBCA) (1) was cross-linked to two cysteines in PDZ2. (*B*) Amino acid sequence of the second PDZ domain in human tyrosine-phosphatase 1E (hPTP1E). A His tag with a HRV 3C cleavage site (blue) was used for purification and cleaved before measurements. The cleavage site is marked with an apostrophe and the two Cys (S21C and E76C) that served as anchor points for the photoswitch are shown in red.

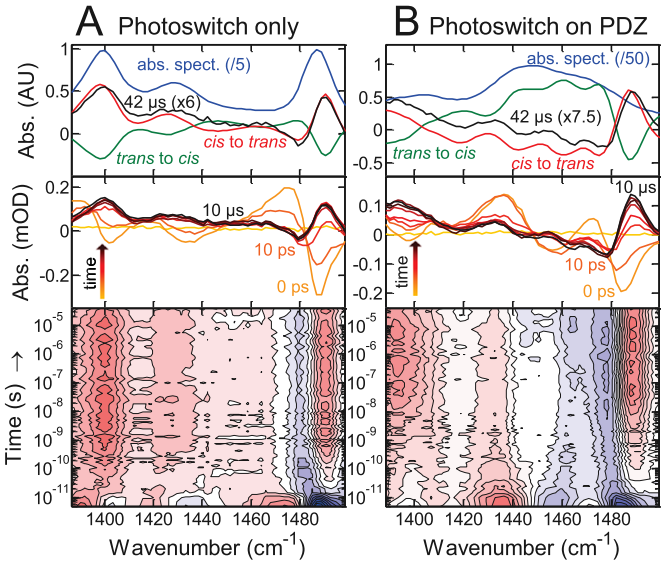

Fig. S2. IR spectra of the ring-mode (~1,390 cm^{-1}) and Amide II (~1,490 cm^{-1}) bands from the photoswitch. (*A* and *B*) (*Top*) Absolute (blue) and difference FTIR spectra (red and green) compared with the transient spectrum at 42 µs (black). (*Middle*) Transient spectra, at −1 ns (yellow), 0 s (light orange), and from 10 ps to 10 µs by decade (orange to black). (*Bottom*) Contour plot of the IR response. (*A*) Photoswitch alone; (*B*) photoswitch on PDZ2.

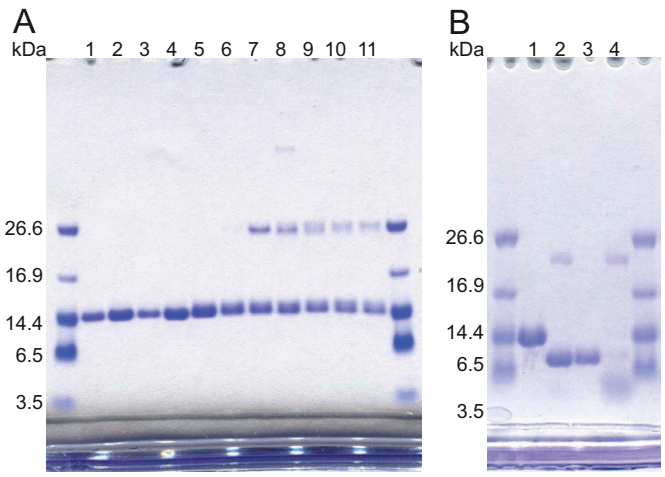

Fig. S3. SDS/PAGE analysis of linking the photoswitch (BSBCA) to PDZ2. Shown are 12% Bis-Tris gels (Novex NuPAGE; Invitrogen) with polypeptide SDS/PAGE molecular weight standards (Bio-Rad) Coomassie stained with Rotiphorese Blue R (Carl Roth GmbH). (*A*) After purification with a MonoQ anion exchange column (GE Healthcare Life Sciences). Lanes 1–5: PDZ2 with the photoswitch correctly linked to the two Cys (mass verified by ESI mass spectrometry). Lanes 6–11: Mixtures of incorrectly linked PDZ2 (monomers with two linkers, dimers, trimers). (*B*) Cleaving of the His tag. Lane 1, before cleaving; lane 2, after cleaving; lane 3, after cleaving and purification with HisTrap column (GE Healthcare Life Sciences); lane 4, HRV 3C protease and free His tag eluted from the HisTrap column.

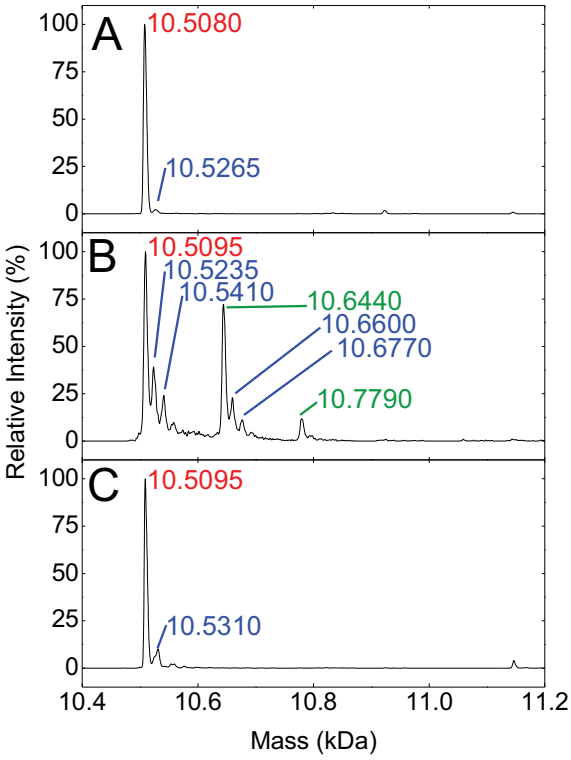

Fig. S4. Mass spectra of PDZ2 linked to the photoswitch. The peak corresponding to the expected mass is labeled in red, peaks originating from the oxidized sample are in blue, and peaks with an additional modification (+135 Da) are in green. (*A*) Before a time-resolved IR measurement, in 50 mM Tris·HCl, 150 mM NaCl, pH 8.5. (*B*) After a time-resolved IR measurement, in 50 mM Tris·HCl, 150 mM NaCl, pH 8.5. (*C*) After a time-resolved IR measurement, in 50 mM borate buffer, 150 mM NaCl, pH 8.5, and under exclusion of oxygen.

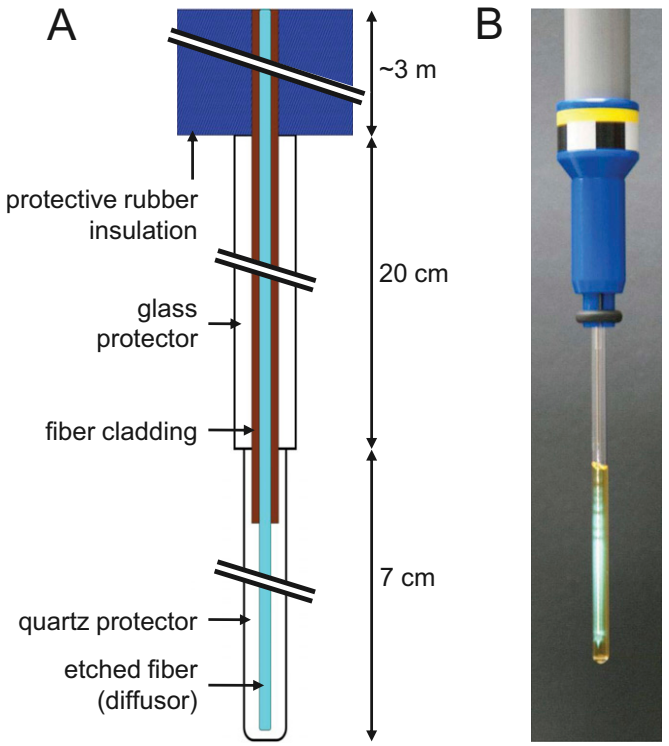

Fig. S5. Illumination of NMR sample. (*A*) Sketch of the NMR inline radial illumination probe (Polymicro Technologies). (*B*) Illumination of a sample in an NMR tube.

Table S1. Complete set of fit parameters for the black lines in Fig. 3

Probe wavenumber	a_0	a_1	τ_1	a_2	τ_2	β	a_3	τ_3
1,491 cm^{-1}	0.12	−0.16	0.015	−0.10	7.3	0.49	0	—
1,640 cm^{-1}	−0.07	0.0	0.015	0.09	7.3	0.49	−0.07	20,000

Amplitudes are in units of mOD (optical density), and time constants are in nanoseconds.

Table S2. Restraints for NMR structure calculation

Type	*cis*	*trans*
NOE	877	992
Photoswitch	2	29
Dihedral restraints	146	145
HN-RDCs		
Pf1	78	80
C12E5	76	76

Table S3. NMR structure statistics

Structural parameters of 20 NMR conformers	*cis*	*trans*
Pairwise cartesian rmsd, Å		
Global backbone heavy atoms	1.02	1.15
Global all heavy atoms	1.39	1.54
Ordered backbone heavy atoms	0.35	0.33
Ordered all heavy atoms	0.92	1.04
Ramachandran quality parameters, %		
Residues in most favored regions	86.7	86.3
Residues in allowed regions	11.2	8.8
Residues in additionally allowed regions	1.8	4.6
Residues in disallowed regions	0.3	0.3
Average rms deviation from current reliable structures, rms *Z*-scores		
Bond lengths	1.050	1.126
Bond angles	1.155	1.187
Omega angle restraints	1.303	1.486
Side-chain planarity	0.447	0.676
Improper dihedral distribution	0.908	0.983
Inside/outside distribution	0.951	0.986
Average deviation from current reliable structures, *Z*-scores		
First-generation packing quality	−1.833	−2.479
Ramachandran plot appearance	−2.014	−2.217
Chi-1/Chi-2 rotamer normality	−3.735	−3.859
Backbone conformation	−0.916	−0.916

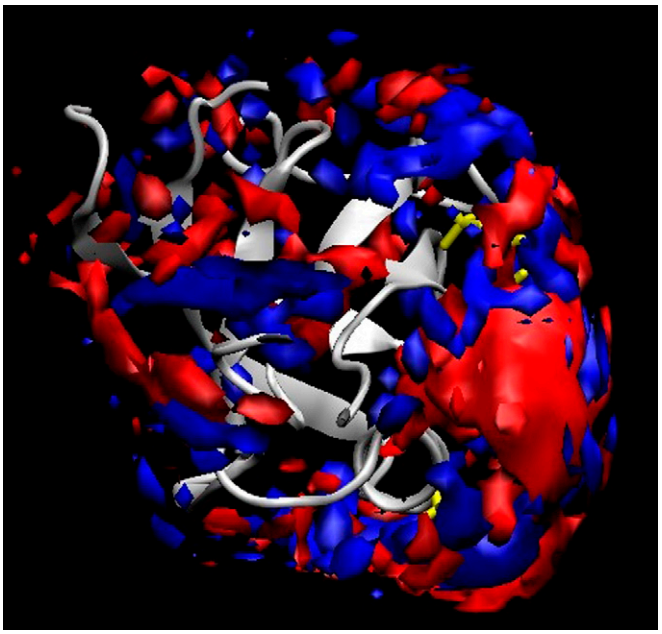

Movie S1. Change of water density after photo-switching the azobenzene moiety that cross-links the binding groove of the PDZ2 domain. Red depicts increased water density; blue depicts decreased water density. The protein is shown by a gray ribbon; the photoswitch (visible only in part) is shown in yellow. The perturbation of the water network on the protein surface propagates within 100 ns around the protein. See Fig. 5 for details.

Movie S1